Preprint Cambridge Centre for Computational Chemical Engineering ISSN 1473 – 4273

Surface properties of heterogeneous polycyclic aromatic hydrocarbon clusters

Kimberly Bowal[1], Laura Pascazio[1], Hongyu Wang[2], Dongping Chen[2], Markus Kraft[1,3,4]

released: 7 November 2019

[1] Department of Chemical Engineering and Biotechnology
University of Cambridge
West Site, Philippa Fawcett Drive
Cambridge, CB3 0AS
United Kingdom
E-mail: mk306@cam.ac.uk

[2] Department of Mechatronical Engineering
Beijing Institute of Technology
Beijing, 100081
China

[3] Cambridge Centre for Advanced Research and Education in Singapore (CARES)
CREATE Tower, 1 Create Way
Singapore, 138602

[4] School of Chemical and Biomedical Engineering
Nanyang Technological University
62 Nanyang Drive
Singapore, 637459

Preprint No. 252

UNIVERSITY OF CAMBRIDGE

Keywords: surface properties, soot particle, reactive site density, alpha, heterogeneous PAH cluster

Edited by
Computational Modelling Group
Department of Chemical Engineering and Biotechnology
University of Cambridge
West Site, Philippa Fawcett Drive
Cambridge, CB3 0AS
United Kingdom

Fax: + 44 (0)1223 334796
E-Mail: c4e@cam.ac.uk
World Wide Web: http://como.cheng.cam.ac.uk/

Abstract

In this paper we investigate the impact of molecular inhomogeneity on the surface properties of soot particles. Using replica exchange molecular dynamics and solvent-excluded surface analysis, we evaluate detailed surface properties directly from particles containing polycyclic aromatic hydrocarbon molecules of different sizes. The temperature-dependent behaviour of surface roughness and number densities of reactive sites are evaluated for particles from 1-5 nm in diameter. The percentage of carbon atoms and zig-zag sites on the particle surface are found to be independent of molecular composition, while molecule heterogeneity influences the accessible hydrogen atoms and free-edge sites. These relationships allow the prediction of surface composition for a given particle diameter. The surface densities of carbon and hydrogen atoms are explained by the morphological changes and molecule size contributions for solid-like and liquid-like configurations. Small molecules contribute significantly to the particle surface properties at low temperatures, regardless of the proportion of molecule sizes, which results in an increased density of accessible carbon atoms for heterogeneous particles. Interestingly, the surface density of edge carbon atoms and free-edge sites can be predicted from the average molecule size alone. The density of hydrogen atoms on the surface follows the average expected values from the constituent molecule sizes, suggesting that for particles containing many different molecule sizes the α parameter corresponding to the HACA mechanism converges to a linear temperature-dependent trend. This quantitative evaluation of the accessibility of reactive sites for heterogeneous particles provides important information for understanding soot particle growth and oxidation.

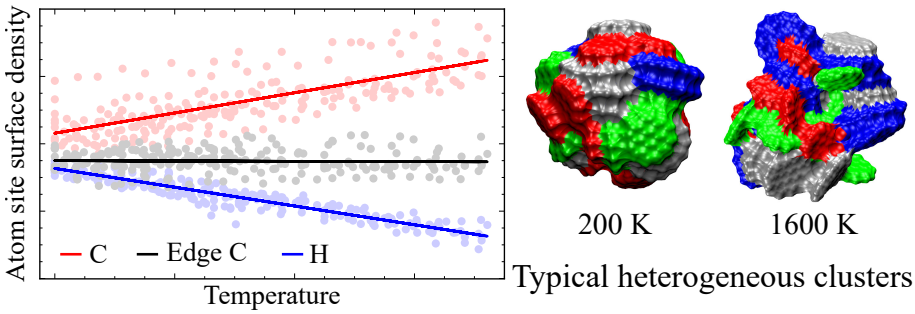

Typical heterogeneous clusters

Highlights:

- Surface composition, roughness, and site densities are explained in the context of cluster morphology.
- Surface densities of hydrogen, internal carbon, and zig-zag sites are dependent on temperature, while edge carbon and free-edge site surface densities can be predicted from average molecule size.
- Small molecules contribute more to cluster surface properties than large molecules.
- The surface area contribution from hydrogen shows a linear temperature-dependent trend with increasing molecular heterogeneity.

Contents

1 Introduction

Soot has an adverse effect on combustion efficiency, human health, and the environment, providing industrial and societal motivation to study its properties and behaviour [17]. The size and nature of soot particles produced in combustion processes are dependent on their mass growth and oxidation, which are governed by chemical interactions between the soot particle surface and gaseous species such as acetylene and oxygen [8, 12]. These surface reactions have been investigated in numerous experimental and theoretical studies and it is well-established that the nanostructures of soot particles, defined by the size, orientation, and organisation of constituent polycyclic aromatic hydrocarbons (PAHs), play a significant role in reactivity [15, 22]. This is due to the influence of nanostructure on the accessibility of reactive sites on the particle surface. Edge carbon (EC) atoms on the rim of PAH molecules have significantly higher reactivities (10-100 fold difference) than internal carbon (IC) atoms on the basal plane [3]. This is because EC atoms can more easily form bonds due to the availability of unpaired sp^2 electrons, where IC atoms share π electrons in chemical bonds [20]. Smaller PAHs possess higher proportions of EC atoms and lower C-to-H ratios, leading to an inverse relationship between molecule size in soot particles and the apparent oxidation rate constant [28].

To capture the dynamic reactivity of soot particles in combustion processes the description of surface reactions involves an empirical parameter α, which captures the fraction of the soot surface available for surface reactions. The parameter α was first introduced by Frenklach and Wang to reproduce soot volume fractions for both high and low temperature flames [14]. The parameter α is often understood to capture the changing morphology of soot particles as a function of temperature and particle size, in particular the presence of reactive graphitic edges or unreactive basal aromatic planes on the particle surface [5]. Due to the difficulty of probing atomic properties with experimental methods, the parameter α is selected to provide the best fit between model predictions and experimental results. As a consequence, this steric parameter is not derived from soot nanostructures, leading to a variety of α values across models without a clear convergence with temperature or over time [9]. Over the last three decades significant attention has been spent to develop improved formulations of the parameter α , including explicit dependencies on temperature [18], particle size [5], and age [25]. Recently, Frenklach presented a new form of α that moves away from variable empiricism and captures instantaneous surface site concentration [13].

Developing a deeper understanding of particle reactivity requires detailed investigation of soot surface properties. Recent modelling work used atomic simulations to characterise the surface properties of PAH clusters and their interactions with gaseous molecules [9, 10, 16]. This provides a numerical basis to connect molecular arrangement with the surface roughness, number density of reactive site i on the surface (χ_i), and a formulation of α that includes the effects of temperature, particle size, and chemical composition. This work is valuable but is limited to homogeneous particles in which there is only one constituent molecule type. Soot particles contain molecules of many sizes which are known to partition in a core-shell structure where the larger molecules make up the particle core (nascent soot) or where larger molecules dominate the outer particle shell (mature soot) [6, 7]. These nanostructural differences are expected to influence particle surface compo-

sition but their detailed effect on χ_i values and the parameter α have yet to be determined.

In this work we provide a detailed numerical evaluation of the surface properties of heterogeneous clusters containing PAHs of different sizes and ratios. This provides insight into the reactive surface of soot particles and allows refinement of model parameters especially important in understanding soot surface growth. The proportion of atom and site types on the particle surface is explored as a function of diameter to highlight the impact of inhomogeneity. Surface roughness and site surface densities are explored, and the contributions of different molecule sizes are highlighted.

2 Methodology

The particle systems investigated are made up of pyrene (PYR), coronene (COR), ovalene (OVA), and circumcoronene (CIR) molecules, which span the molecular sizes observed experimentally in soot particles [4, 6]. Binary and quaternary particles of various sizes, containing two and four molecule types respectively, are considered (listed in Table 1). Two types of binary clusters, containing CIR and COR or OVA and PYR, are examined. Two types of quaternary clusters are also considered, one containing a uniform distribution of molecule types and the other with a nonuniform distribution in which the larger molecules are found in higher proportions. This latter distribution is selected as a conservative case for surface property analysis, since smaller molecules are expected to contribute more significantly due to core-shell partitioning [7]. The molecule types are shown in Figure 1 along with snapshots of representative quaternary and binary particles at low and high temperatures.

Table 1: *Heterogeneous particles considered in this work. Systems labelled by an asterisk were taken from Ref. [7].*

Cluster type	**Number of molecules**	**Particle diameter (nm)**
Binary 50% OVA, 50% PYR	4	1.34
	32*	2.80
	100*	4.15
Binary 50% CIR, 50% COR	4	1.54
	32*	3.20
	100*	4.78
Quaternary (uniform) 25% CIR, 25% OVA, 25% COR, 25% PYR	4	1.45
	32	3.02
	100*	4.48
Quaternary (nonuniform) 40% CIR, 30% OVA, 20% COR, 10% PYR	10	2.11
	24	2.87
	100	4.70

Heterogeneous particles are produced following the same procedure as our previous work [7]. PAH clusters are generated by randomly placing molecules in a spherical volume

using the PACKMOL software [21]. A two-step minimisation process using the steepest descent and low-memory Broyden-Fletcher-Goldfarb-Shanno algorithms removes excess energy prior to the equilibration and production simulations. Replica exchange molecular dynamics (REMD) simulations are performed using Gromacs 5.1.4 [1]. REMD simulations use a large number of interacting parallel simulations to rapidly determine stable structures across a large range of temperatures. In this work, a timestep of 1 fs is used and 1 ns simulations are sufficient for particles < 3 nm while larger clusters (up to 5 nm) require 2 ns simulations to produce structurally equilibrated particles with energy drifts less than that of experimental error. To capture solid-like and liquid-like particle morphologies, clusters are simulated across wide temperature ranges: 200 - 800 K for particles containing OVA and PYR, 400 - 1600 K for CIR and COR particles, and 200 - 1600 K for all quaternary systems. This requires between 14 and 88 REMD replicas to maintain an acceptable replica exchange acceptance with attempted exchanges every 100 fs. A spherical position potential is applied and intermolecular interactions are described using the isoPAHAP potential [26], parameterised specifically for PAH interactions.

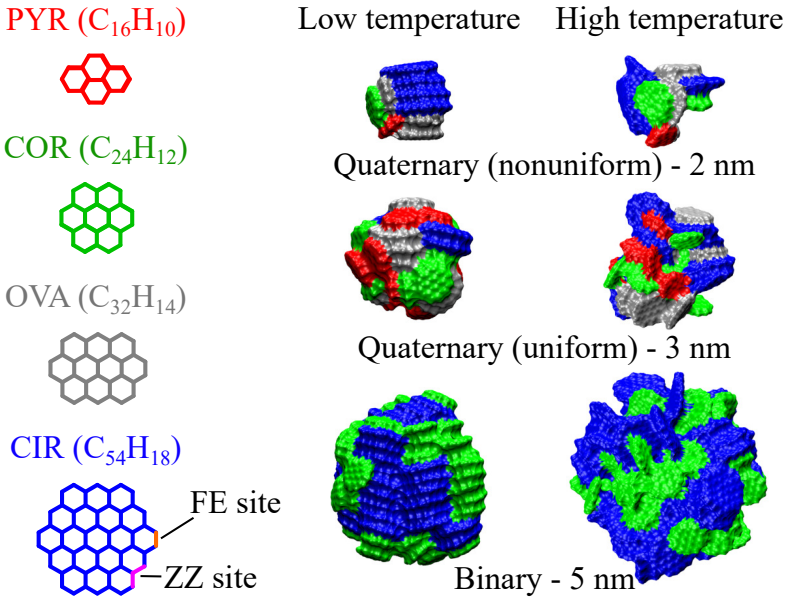

Figure 1: *Pyrene (red), coronene (green), ovalene (grey), and circumcoronene (blue) molecules are considered in this work. Example free-edge and zig-zag sites are highlighted. Snapshots of representative heterogeneous particles are shown at low and high temperatures (solid-like and liquid-like configurations, respectively).*

The detailed surface properties of the simulated particles are determined using solvent-excluded surface (SES) analysis, which uses a 'rolling ball' algorithm to describe the three-dimensional surface. This provides the surface area and quantitative contributions from reactive sites of interest: hydrogen (H) and carbon (C) atoms, the latter of which can be split into IC atoms and EC atoms. EC atoms can be further defined as free-edge (FE) sites containing two carbon atoms or zig-zag (ZZ) sites made up of three carbon atoms, shown in Figure 1. Statistics for the detailed surface properties are collected from 6 equilibrated configurations, each extracted at 20 temperatures. Following a previous

work on homogeneous particles [9], the SES analysis uses the MSMS 6.2.1 program [24] with a probe radius of 2.0 Å, corresponding to an interacting acetylene molecule.

3 Results

3.1 Percent on surface

A key feature of soot surface analysis involves understanding the proportion of potential reactive sites in the particle that are accessible to a species interacting with the surface. Figure 2 shows the percentage of each atom or site type present on the particle surface as a function of the particle diameter. This allows us to predict the number of reactive surface sites based on particle size, given the total number of atoms or sites in the system. These results are shown for solid-like configurations, and similar trends are seen for higher temperatures, with percent values increasing by $3-4\%$ from solid-like to liquid-like morphologies.

All particles follow a size-dependent trend for surface C atoms and ZZ sites, decreasing from around 55 to 12% and 35 to 5%, respectively. These curves follow a reciprocal diameter trend, indicating that the surface area to volume ratio captured in these values is a controlling factor. This shows that these values are independent of molecular composition, and thus 'real' soot particles can be simplified as homogeneous models. The percent values of H atoms on the surface are significantly higher than C atoms since the solid-like configuration of PAH clusters promotes π-stacking where the molecule edges face outwards, seen for a small heterogeneous particle in Figure 3. The proportion of H atoms on the surface shows an added dependence on molecule type, with larger constituent molecules providing larger percentages of surface H values, indicated by an arrow in Figure 2(b). This spread can be attributed to differences in stack sizes for the different molecule types. The dissociation energy required to split a PAH stack into two stacks increases with the increasing molecule size, so that stacks are favoured until a length approximately equal to the constituent molecule length [23]. Therefore a particle containing smaller molecules contains a larger number of short stacks, corresponding to increased disorder and more hydrogen atoms hidden in the bulk, than a particle of the same diameter containing larger molecules. The percentage of FE sites on the particle surface is influenced by the presence of different molecule sizes, with heterogeneous particles presenting significantly higher values ($33-96\%$ for the particle sizes studied here) than homogeneous systems ($5-19\%$). This can be largely attributed to the molecule stacking behaviour. In homogeneous particles the PAHs form aligned stacks and therefore the carbon contributions come predominantly from the molecules capping the ends of the stacks. Heterogeneous particles also form π stacks but the different molecule sizes allow greater accessibility of FE sites for heterogeneous particles compared to homogeneous stacking. For example, the top view of the small heterogeneous particle in Figure 3 shows how FE sites on the larger molecules contribute to the particle surface so that 95% of the FE sites are found on the surface. In contrast, the ZZ sites on the surface show the same trends for both homogeneous and heterogeneous particles, again with a typical surface area/volume curve. This is because the molecule size differences are not large enough to reveal the

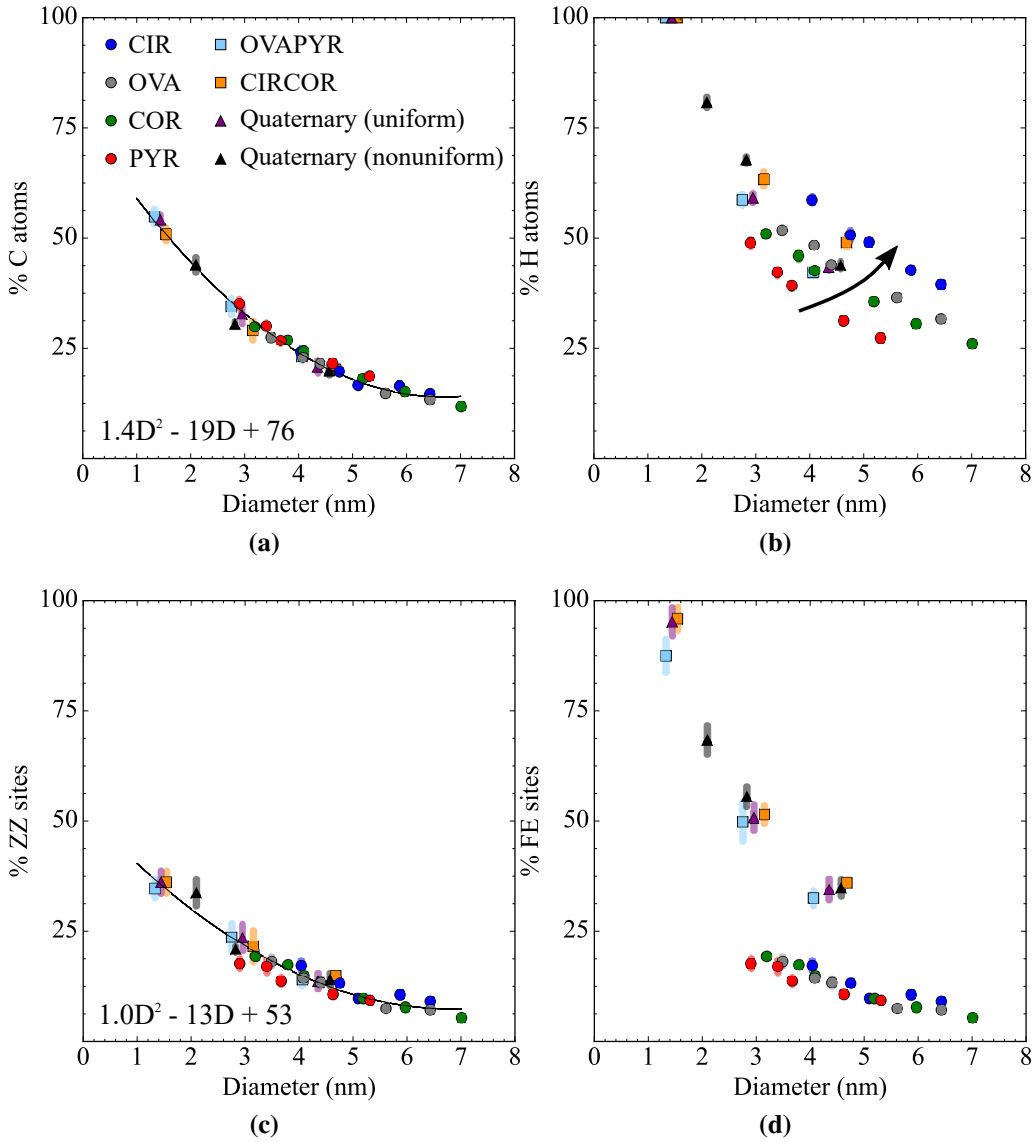

Figure 2: *Percentage of (a) carbon atoms, (b) hydrogen atoms, (c) ZZ sites, and (d) FE sites present on the particle surface for homogeneous and heterogeneous particles at solid-like configurations. Shaded areas indicate the standard deviation. The arrow in (b) indicates the effect of increasing molecule size. Homogeneous particle values are taken from Ref. [10].*

central carbon atoms required for the 3-atom ZZ sites. For example, Figure 3 shows that the only inner EC atoms (shown in blue) accessible to the surface probe for the smallest uniform quaternary particle are within the top and bottom molecules in the stack. It is also worth noting that since each molecule contains six FE sites, the percentage of FE sites is dependent on the total number of molecules rather than the particle diameter, seen by the grouping of heterogeneous particles FE site percentages across diameters.

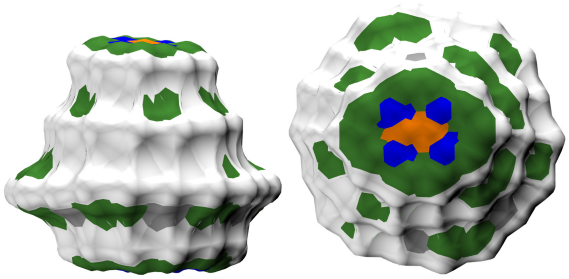

(a) *Side view* **(b)** *Top view*

Figure 3: *Snapshots of the probe-accessible surface of a 1.45 nm quaternary (uniform) particle in its solid-like state. FE sites, internal ZZ carbon atoms, hydrogen atoms, and IC atoms are coloured green, blue, white, and orange, respectively. This particle has 100% of the H atoms, 54% of the carbon atoms (72% of the edge, 19% of the non-edge), 95% of the FE sites, and 36% of the ZZ sites on the particle surface.*

3.2 Particle roughness

Particle roughness is calculated as the ratio of the SES surface area to the spherical-equivalent surface area, shown for all heterogeneous particles in Figure 4. In all cases roughness increases consistently with temperature. This is unsurprising because increasing thermal energy causes molecules to be more mobile and change from their low temperature configuration of parallel stacks to a more disordered configuration in which surface pockets are present [10].

Although no single relationship can describe the surface roughness of all particles across temperatures, it is clear that the particle size is an important factor: as the particle diameter increases, its roughness increases. In other words, the larger the particle, the less spherical it is. The proportion of molecules is less important, and the roughness of binary or quaternary particles (either in uniform or nonuniform molecular ratios) is similar. It is interesting to note that at smaller particle sizes, the constituent molecule type provides some contribution as well. This is seen in the increased roughness of the ≤ 3 nm OVAPYR particles compared to their CIRCOR counterparts despite their smaller particle size. This is likely due to the higher rim-to-plane area and elliptical shape of OVA and PYR molecules. All heterogeneous particles follow the same trends and the molecular composition does not play a significant role. This suggests that at low temperatures 'real' soot particles would have a surface area that is 10-30% higher than a spherical approximation would provide, and may be closer to 160% higher for particles > 4 nm at high temperatures.

3.3 Surface composition

Temperature has a direct effect on soot particle morphology and therefore influences surface reactivity. Figure 5 shows χ_i values (calculated as the number of i reactive sites on

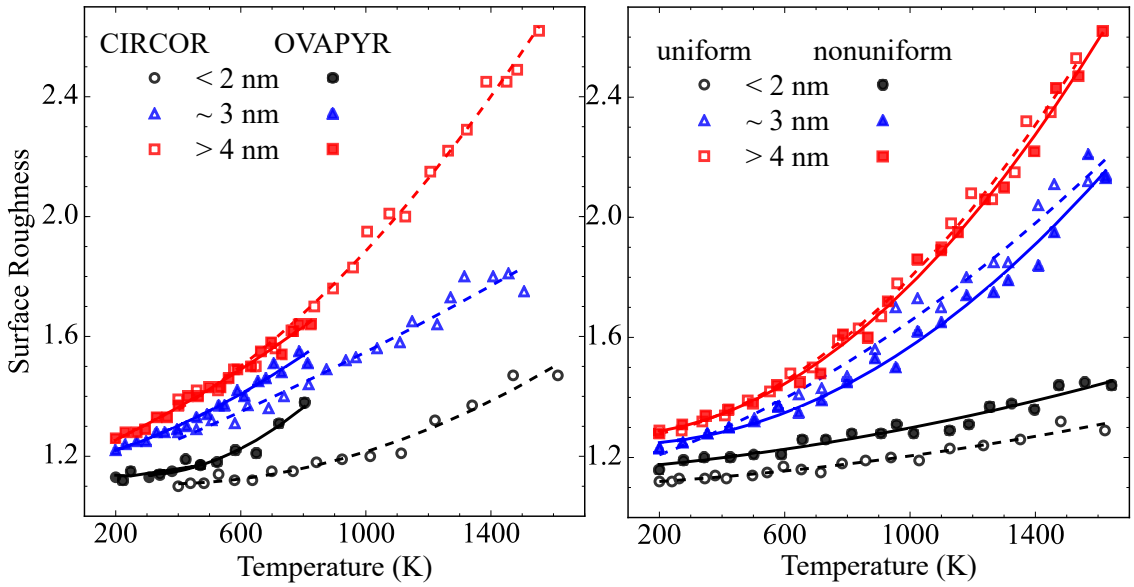

(a) *Binary particles* **(b)** *Quaternary particles*

Figure 4: *Surface roughness of binary and quaternary particles with increasing temperature. The smallest particles (diameter* < 2 *nm) are shown with black circles, intermediate particles (diameter* $\approx$ *3 nm) are blue trianges, and the largest particles (diameter* > 4 *nm) are red squares. Filled and open symbols refer to OVAPYR and CIRCOR particles, respectively, for the binary cases and uniform and nonuniform molecule ratios, respectively, for the quaternary particles. Lines are provided to guide the eye.*

the surface over the total SES area) for all particle types and sizes studied in this work. Scatter points show individual heterogeneous particles, with lines indicating the overall trends. The behaviour of homogeneous particles are provided with dashed trend lines. All systems show the same surface density trends with increasing temperature: χ_C and χ_{ZZ} increase, while χ_H and χ_{FE} decrease. These temperature-dependent behaviours can be explained by the change from solid-like to liquid-like particle morphology and the consequential contribution of different molecule types.

The decrease of χ_H with increased temperature, and the corresponding increase in χ_C, are expected consequences of the morphology changes. Low temperature particles consist of stacked PAHs with molecule edges aligned with the particle surface, so that hydrogen atoms make up a significant portion of the surface. At increased temperatures, the stacks break up and the molecule planar surfaces are exposed to the surface, providing a significant increase in particle surface area of which the majority is contributed from IC atoms. This is visible in the snapshots of solid-like and liquid-like particles in Figure 1. The χ_C and χ_H are primarily dependent on temperature, with consistent values across particle diameters, molecule sizes, and component ratios. For homogeneous particles, separate trend lines are present for each of the molecule types as a consequence of their temperature-dependent behaviour. These homogeneous particle χ_i value differences are a result of reporting as a function of the absolute temperature, since molecule mobility

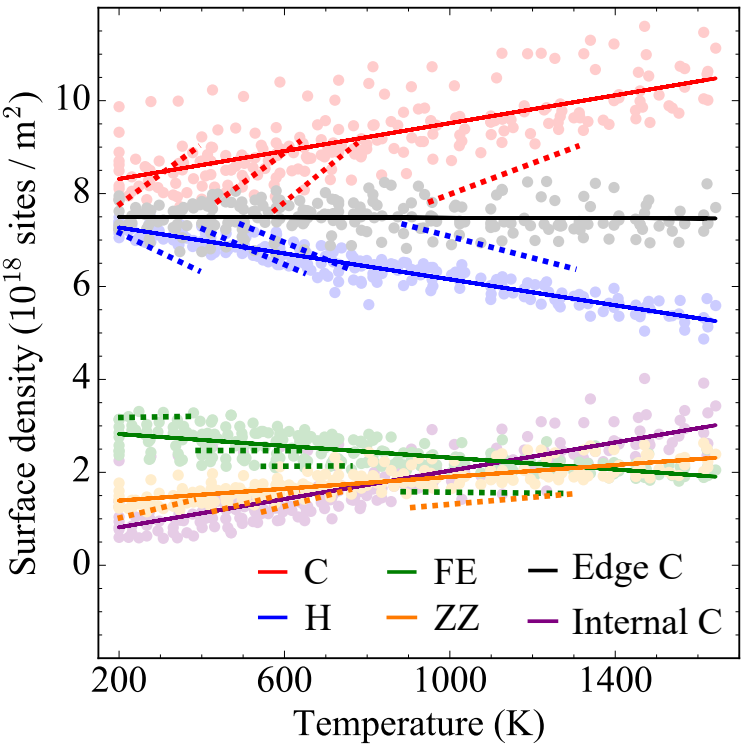

Figure 5: *Surface densities of atom types and reactive sites across a range of temperatures for all heterogeneous particles. Surface densities of homogeneous particles, taken from Ref. [10], are shown with dashed lines. All lines are provided to guide the eye.*

at a given temperature is dependent on the molecule size. Describing these properties with reduced temperature values would produce aligned χ_i values, but this is unfeasible at the moment since heterogeneous melting points for comparison are not known. Mixing molecule sizes in the heterogeneous particles provides single moderate trends.

χ_C shows a relatively large variance and so the contributions from carbon types are investigated further. Isolating the surface density contributions shows that the increase in χ_C with temperature is driven by the IC atoms, while χ_{EC} does not change significantly with temperature. To be clear, the number of sites on the surface increases for all site types as temperature increases (except when the percent of surface H atoms is already at 100% for some of the < 2 nm particles). However, their magnitude increase compared to the increase in particle surface area with temperature determines the density temperature response. In this way, χ_{EC} remains consistent with temperature since the increase in EC atoms corresponds to the increase in surface area. Interestingly, χ_{EC} can be described by the molecular composition alone. As the constituent molecule size increases, the contribution of EC atoms to the particle surface decreases, leading to the following relationship: $\chi_{EC} = -4.9L + 10$, where L is the average molecule length. χ_{FE} shows the same behaviour, indicated by different temperature-independent densities for the four homogeneous particle compositions in Figure 5. This is discussed in more detail in the Supplementary Material.

3.4 Molecule type contributions

Taking a closer look at the individual molecule types, the same increasing and decreasing atom and site trends seen in Figure 5 are observed with increasing molecule size. This suggests that there is an increasing surface contribution from larger molecules on the surface as temperature increases. Figure 6 shows the contributions of different molecule types to the total carbon and hydrogen atoms present on the surface for particles with a diameter of approximately 3 nm, at low and high temperatures corresponding to solid-like and liquid-like particles, respectively. These percent values are normalised by the expected contributions taking into account the proportion provided by each molecule. At solid-like

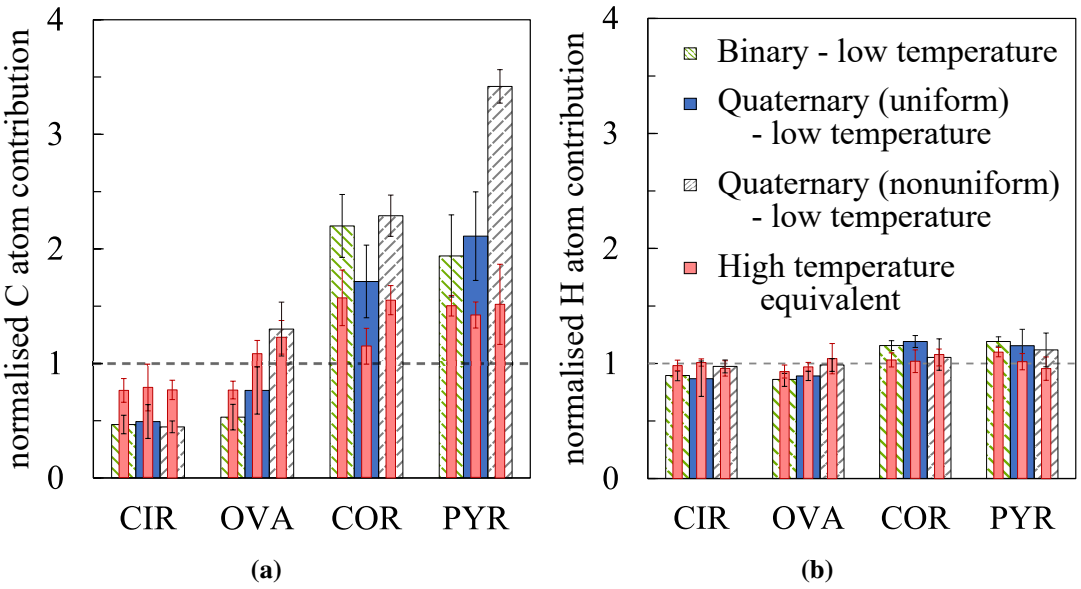

Figure 6: *Molecule type contributions to the carbon and hydrogen atoms on the surface of 3 nm particles. Low temperature values provide solid-like particles, and the corresponding liquid-like particles at high temperatures are shown with inset narrow red bars. All values are normalised by the expected values considering molecule type proportions.*

configurations, the surface carbon atoms experience higher contributions from the small molecules than expected from the molecular proportions. This can be explained by the core-shell configuration at low temperatures [7]. The two types of binary particles (CIR-COR and OVAPYR) show half of the expected contribution from the larger molecules (CIR or OVA) and double the expected contribution from the smaller molecules (COR or PYR). The quaternary particles show the same behaviour, with increasing contributions from decreasing molecule sizes. The difference between uniform and nonuniform quaternary particles highlights the presence of small molecules on the particle surface. Nonuniform particles have higher normalised values for the small molecules since the lower proportion of small molecules in these systems would be expected to play a smaller role in the surface composition. These results show that small molecules are present on the particle surface regardless of the distribution of molecules sizes in the particle. At

high temperatures the molecule size differences decrease towards their expected molecular contributions, corresponding to a mixed arrangement in which all of the molecule types contribute proportionately to the surface properties. In contrast, all molecule types contribute proportionately to the surface H atoms in solid-like and liquid-like configurations.

3.5 Alpha

The parameter α provides a reactivity factor that accounts for temperature-dependent sterics, due to the increasing molecule mobility with increasing temperature, which causes molecules to break the stacked structure that exposes hydrogen atoms to the surface and introduces more unreactive basal planes, as well as the increasing contribution of larger molecules. In this work, the parameter α is defined as the area of hydrogen atoms over the total SES area. Figure 7 shows α values for a series of 3 nm particles containing different molecule types. As with the χ_H values, there are distinct downward trends for each homogeneous particle type with temperature. Interestingly, increasing heterogeneity converges the α parameter to a similar temperature dependence, which can be approximated by a simple linear temperature-dependent relationship. The heterogeneous particles show α values consistent with a weighted average of the molecular components, suggesting that the increasing heterogeneity of 'real' soot particles produces a consistent trend. The same behaviour is seen for particles $>$ 4 nm, included in the Supplementary Material.

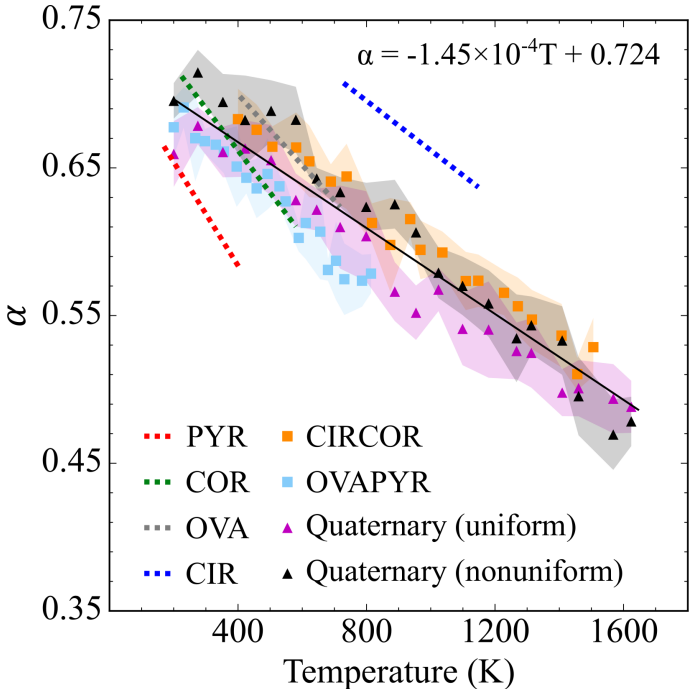

Figure 7: *Parameter α for 3 nm particles as a function of temperature. Shaded areas show the standard deviation of heterogeneous particle values. Homogeneous particle values, taken from Ref. [10], are shown as dashed lines. A single trend line is shown for all of the heterogeneous cases.*

This work forms a foundation for understanding how heterogeneity in molecule size influences the surface properties of soot particles. Further work can explore the influence of complex molecule types believed to play a role in soot, such as PAHs with crosslinks, aliphatic chains, or curvature [11, 19], in surface properties. For example, increasing curvature is seen to substantially increase oxidative reactivity but it is unknown to extent this is due to the individual molecule reactivity or a consequence of an altered nanostructure of particles containing curved aromatic molecules [27].

4 Conclusions

PAH particles containing two or four molecule types are studied to provide insight into the effect of molecular heterogeneity on soot particle surface properties. A thorough analysis is conducted across particle sizes (1-5 nm) and temperatures (200-1600 K). Relationships between particle diameter and the percentage of reactive sites on the particle surface are identified, showing that C atom and ZZ site percentages do not change with heterogeneity. Molecule size differences in heterogeneous particles increase the FE sites available for reactions, while H atom percentages increase with constituent molecule size. Particle roughness increases with temperature and particle size, with particle composition playing a secondary role. The controlling parameters for surface densities of reactive sites are also identified, showing that χ_{H}, χ_{IC}, and χ_{ZZ} are dependent on temperature while χ_{EC} and χ_{FE} can be predicted from the average molecule length. These trends are influenced by enhanced surface contributions from small molecules at low temperatures. Finally, the temperature-dependent behaviour of the parameter α shows a correlation to constituent molecule size, suggesting that the α parameter for heterogeneous particles converges to an average value of the constituent molecules.

Acknowledgments

This work used the ARCHER UK National Supercomputing Service (http://www.archer.ac.uk). K.B. is grateful to the Cambridge Trust and the Stanley Studentship at King's College, Cambridge for their financial support. D.C. acknowledges the support of the National Natural Science Foundation of China (No. 51806016) and the Beijing Institute of Technology Research Fund Program for Young Scholars. This project is also supported by the National Research Foundation, Prime Minister's Office, Singapore under its Campus for Research Excellence and Technological Enterprise programme.

A Supplementary Material

A.1 Surface densities of edge carbon atoms and free-edge sites

The density of edge carbon atoms on the particle surface, χ_{EC}, is not affected by temperature or particle size, and can therefore be described by the molecular composition alone. As seen in Figure S1(a), the contribution of edge carbon atoms to the surface decreases as the constituent molecule size increases, with homogeneous circumcoronene, ovalene, coronene, and pyrene particles presenting values of approximately 3.5×10^{18}, 4.6×10^{18}, 5.2×10^{18}, and 6.7×10^{18}, respectively. A weighted average of these values provides a good prediction of heterogeneous particles examined in this work (for example, a CIR-COR particle is an average of CIR and COR values), leading to the simple linear trend shown in Figure S1(b). This relationship allows us to estimate the density of edge carbons on the particle surface from an average molecule length value, such as that determined by fringe analysis of high resolution transmission electron microscopy images. As an example, Ref. [2] gives an average fringe length value of 0.80 nm for young soot produced in a benzene flame. We can estimate that these particles have a surface density of 6.1×10^{18} atoms of edge carbon per m^2.

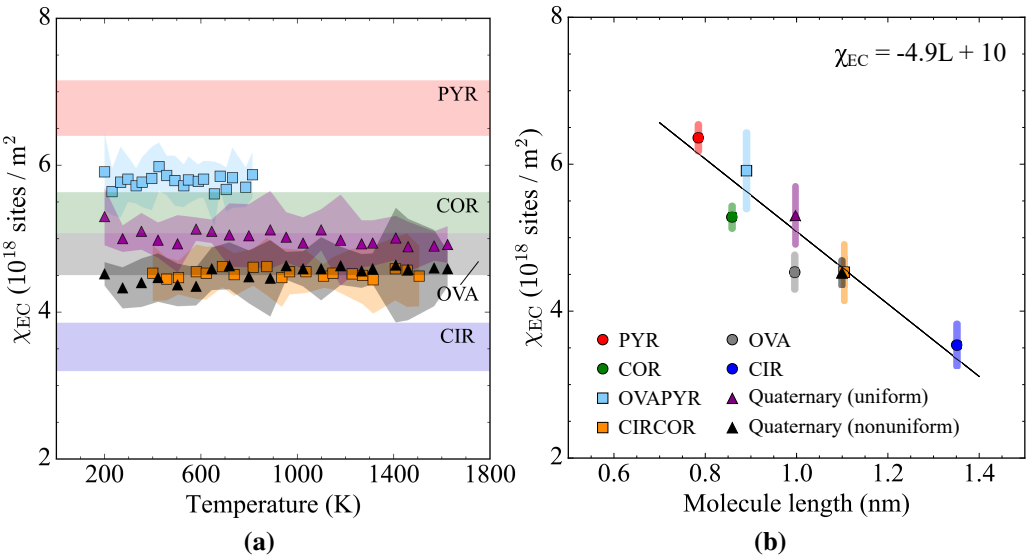

Figure S1: *Edge carbon atom density on the particle surface, χ_{EC}, as a function of the temperature (a) and average molecule length, L (b) for particles with a diameter of 3 nm.*

As seen in Figure S2, the surface density of free-edge sites, χ_{FE}, shows similar behaviour, although there is a slight decrease in χ_{FE} with increasing temperature due to the increasing contribution of large molecules to the surface. The linear trend provided relates the surface density of FE sites with the average molecule length.

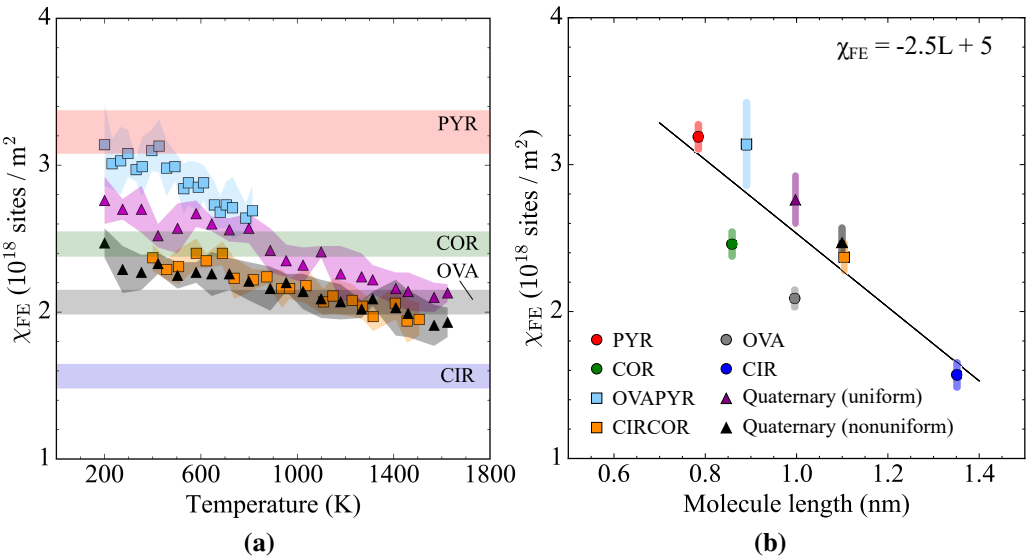

Figure S2: *Free-edge site density on the particle surface, χ_{FE}, as a function of the temperature (a) and average molecule length, L (b) for particles with a diameter of 3 nm.*

A.2 Parameter α for 5 nm particles

The parameter α is strongly dependent on temperature, with particle diameter playing a weaker role. Figure S3 shows values of the parameter α across a wide range of temperatures for homogeneous and heterogeneous particles approximately 5 nm in diameter. As in the 3 nm case reported earlier, the heterogeneous particle α parameter values reflect an average of the homogeneous constituents and simple linear relationship can be used to approximate α of heterogeneous particles as a function of temperature.

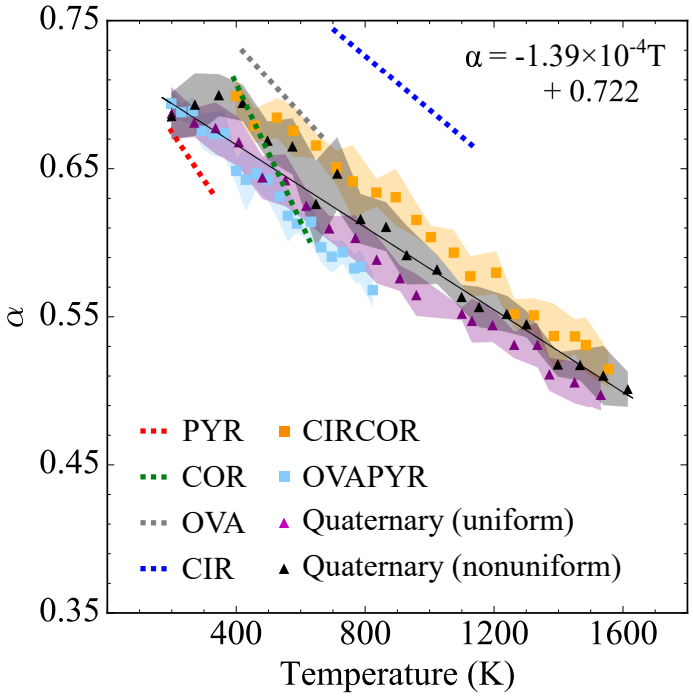

Figure S3: *Parameter α for particles with a diameter of approximately 5 nm as a function of temperature. Shaded areas show the standard deviation of heterogeneous particle values. Homogeneous particle values, taken from Ref. [10], are shown as dashed lines. A single trend line is shown for all of the heterogeneous cases.*

References

[1] M. J. Abraham, T. Murtola, R. Schulz, S. Páll, J. C. Smith, B. Hess, and E. Lindahl. GROMACS: High performance molecular simulations through multi-level parallelism from laptops to supercomputers. *SoftwareX*, 1:19–25, 2015.

[2] M. Alfè, B. Apicella, R. Barbella, J.-N. Rouzaud, A. Tregrossi, and A. Ciajolo. Structure–property relationship in nanostructures of young and mature soot in premixed flames. *Proc. Combust. Inst.*, 32(1):697–704, 2009.

[3] H. Allendorf and D. Rosner. Comparative studies of the attack of pyrolytic and isotropic graphite by atomic and molecular oxygen at high temperatures. *AIAA J.*, 6 (4):650–654, 1968.

[4] B. Apicella, P. Pre, M. Alfè, A. Ciajolo, V. Gargiulo, C. Russo, A. Tregrossi, D. Deldique, and J. Rouzaud. Soot nanostructure evolution in premixed flames by High Resolution Electron Transmission Microscopy (HRTEM). *Proc. Combust. Inst.*, 35(2):1895–1902, 2015.

[5] J. Appel, H. Bockhorn, and M. Frenklach. Kinetic modeling of soot formation with detailed chemistry and physics: laminar premixed flames of C_2 hydrocarbons. *Combust. Flame*, 121(1-2):122–136, 2000. doi:10.1016/S0010-2180(99)00135-2.

[6] M. L. Botero, Y. Sheng, J. Akroyd, J. Martin, J. A. Dreyer, W. Yang, and M. Kraft. Internal structure of soot particles in a diffusion flame. *Carbon*, 141:635–642, 2019.

[7] K. Bowal, J. W. Martin, and M. Kraft. Partitioning of polycyclic aromatic hydrocarbons in heterogeneous clusters. *Carbon*, 143:247–256, 2019.

[8] J. Camacho, Y. Tao, and H. Wang. Kinetics of nascent soot oxidation by molecular oxygen in a flow reactor. *Proc. Combust. Inst.*, 35(2):1887–1894, 2015.

[9] D. Chen and K. H. Luo. Reactive sites on the surface of polycyclic aromatic hydrocarbon clusters: A numerical study. *Combust. Flame*, 211:362–373, 2020. doi:10.1016/j.combustflame.2019.09.034.

[10] D. Chen, J. Akroyd, S. Mosbach, and M. Kraft. Surface reactivity of polycyclic aromatic hydrocarbon clusters. *Proc. Combust. Inst.*, 35(2):1811–1818, 2015.

[11] P. Elvati, K. Turrentine, and A. Violi. The role of molecular properties on the dimerization of aromatic compounds. *Proc. Combust. Inst.*, 37(1):1099–1105, 2019.

[12] M. Frenklach. Reaction mechanism of soot formation in flames. *Phys. Chem. Chem. Phys.*, 4(11):2028–2037, 2002.

[13] M. Frenklach. New form for reduced modeling of soot oxidation: Accounting for multi-site kinetics and surface reactivity. *Combust. Flame*, 201:148–159, 2019.

[14] M. Frenklach and H. Wang. Detailed modeling of soot particle nucleation and growth. *Proc. Combust. Inst.*, 23(1):1559–1566, 1991. doi:10.1016/S0082-0784(06)80426-1.

[15] M. Frenklach, Z. Liu, R. I. Singh, G. R. Galimova, V. N. Azyazov, and A. M. Mebel. Detailed, sterically-resolved modeling of soot oxidation: Role of O atoms, interplay with particle nanostructure, and emergence of inner particle burning. *Combust. Flame*, 188:284–306, 2018.

[16] P. Grančič, J. W. Martin, D. Chen, S. Mosbach, and M. Kraft. Can nascent soot particles burn from the inside? *Carbon*, 109:608–615, 2016.

[17] M. Z. Jacobson. Short-term effects of controlling fossil-fuel soot, biofuel soot and gases, and methane on climate, Arctic ice, and air pollution health. *J. Geophys. Res. Atmos.*, 115(14), 2010. doi:10.1029/2009JD013795.

[18] A. Kazakov, H. Wang, and M. Frenklach. Detailed modeling of soot formation in laminar premixed ethylene flames at a pressure of 10 bar. *Combust. Flame*, 100 (1-2):111–120, 1995. doi:10.1016/0010-2180(94)00086-8.

[19] J. W. Martin, K. Bowal, A. Menon, R. I. Slavchov, J. Akroyd, S. Mosbach, and M. Kraft. Polar curved polycyclic aromatic hydrocarbons in soot formation. *Proc. Combust. Inst.*, 37(1):1117–1123, 2019.

[20] J. W. Martin, D. Hou, A. Menon, J. Akroyd, X. You, and M. Kraft. Reactivity of polycyclic aromatic hydrocarbon soot precursors: Implications of localised π-radicals on rim-based pentagonal rings. *J. Phys. Chem. C*, 143:26673–26682, 2019.

[21] L. Martinez, R. Andrade, E. G. Birgin, and J. M. Martinez. PACKMOL: A package for building initial configurations for molecular dynamics simulations. *J. Comput. Chem.*, 30(13):2157–2164, 2009. doi:10.1002/jcc.21224.

[22] J.-O. Müller, B. Frank, R. E. Jentoft, R. Schlögl, and D. S. Su. The oxidation of soot particulate in the presence of NO_2. *Catal. Today*, 191(1):106–111, 2012.

[23] M. Rapacioli, F. Calvo, F. Spiegelman, C. Joblin, and D. Wales. Stacked clusters of polycyclic aromatic hydrocarbon molecules. *J. Phys. Chem. A*, 109(11):2487–2497, 2005.

[24] M. F. Sanner, A. J. Olson, and J.-C. Spehner. Reduced surface: An efficient way to compute molecular surfaces. *Biopolymers*, 38(3):305–320, 1996.

[25] J. Singh, M. Balthasar, M. Kraft, and W. Wagner. Stochastic modeling of soot particle size and age distributions in laminar premixed flames. *Proc. Combust. Inst.*, 30 (1):1457–1465, 2005.

[26] T. S. Totton, A. J. Misquitta, and M. Kraft. A first principles development of a general anisotropic potential for polycyclic aromatic hydrocarbons. *J. Chem. Theory Comput.*, 6(3):683–695, 2010. doi:10.1021/ct9004883.

[27] R. L. Vander Wal and A. J. Tomasek. Soot oxidation: dependence upon initial nanostructure. *Combust. Flame*, 134(1-2):1–9, 2003.

[28] K. Yehliu, R. L. Vander Wal, O. Armas, and A. L. Boehman. Impact of fuel formulation on the nanostructure and reactivity of diesel soot. *Combust. Flame*, 159(12): 3597–3606, 2012.